

Tunable coupling and isolation of single electrons in silicon quantum dots

H. G. J. Eenink,^{1,*} L. Petit,^{1,*} W. I. L. Lawrie,¹ J. S. Clarke,² L. M. K. Vandersypen,¹ and M. Veldhorst¹

¹*QuTech and Kavli Institute of Nanoscience, TU Delft, P.O. Box 5046, 2600 GA Delft, Netherlands*

²*Components Research, Intel Corporation, 2501 NE Century Blvd, Hillsboro, Oregon 97124, USA*

Extremely long coherence times, excellent single-qubit gate fidelities and two-qubit logic have been demonstrated with silicon metal-oxide-semiconductor spin qubits, making it one of the leading platforms for quantum information processing. Despite this, a long-standing challenge has been the demonstration of tunable tunnel coupling between single electrons. Here we overcome this hurdle with gate-defined quantum dots and show couplings that can be tuned on and off for quantum operation. We use charge sensing to discriminate between the (2,0) and (1,1) charge states of a double quantum dot and show high charge sensitivity. We demonstrate tunable coupling up to 13 GHz, obtained by fitting charge polarization lines, and tunable tunnel rates down to below 1 Hz, deduced from the random telegraph signal. The demonstration of tunable coupling between single electrons in silicon provides significant scope for high-fidelity two-qubit logic toward quantum information processing with standard manufacturing.

Quantum computation with quantum dots has been proposed using qubits defined on the spin states of one [1], two [2] or more [3, 4] electrons. In all these proposals, a crucial element required to realize a universal quantum gate set is the exchange interaction between electrons. The exchange interaction is set by the tunnel coupling and detuning, and gaining precise control over these parameters enables to define and operate qubits at their optimal points [5–8]. Excellent control has already been reported in GaAs [5, 6, 9], strained silicon [10, 11], and more recently in strained germanium [12, 13]. Reaching this level of control in silicon metal-oxide-semiconductor (SiMOS) quantum dots is highly desired as this platform has a high potential for complete integration with classical manufacturing technology [14–16]. However, current two-qubit logic with single spins in SiMOS is based on controlling the exchange using the detuning only [17] or is executed at fixed exchange interaction [18].

In SiMOS, a first step toward the required control to materialize architectures for large-scale quantum computation [1, 19–24] has been the demonstration of tunable coupling in a double quantum dot system operated in the many-electron regime, where gaining control is more accessible owing to the larger electron wave function [25]. More recently, exchange-controlled two-qubit operations have been shown with three-electron quantum dots [26]. However, tunnel couplings between single electrons that can be switched off and turned on for qubit operation, still remain to be shown in SiMOS.

In this work we show a high degree of control over the tunnel coupling of single electrons residing in two gate-defined quantum dots in a SiMOS device. The system is stable and no unintentional quantum dots are observed. We are able to measure charge transitions using a sensitive single-electron-transistor (SET) as charge sensor, and characterize the system in the single-electron regime. From a comparison of charge stability diagrams of weakly

and strongly coupled double quantum dots, we conclude that we control the tunnel coupling by changing quantum dot location. We show that we can effectively decouple the double quantum dot from its reservoir and control the inter-dot tunnel coupling of the isolated system with a dedicated barrier gate. We quantify the tunability of the coupling by analyzing charge polarisation lines and random telegraph signals and find tunnel coupling up to 13 GHz and tunnel rates down to below 1 Hz.

I. RESULTS

Figure 1a shows a scanning electron micrograph (SEM) of a SiMOS device nominally identical to the one measured. A high quality wafer is realized [14] with a 100 nm ²⁸Si epilayer, removing nuclear spin interactions to obtain spins with long quantum coherence [27], covered by 10 nm thermally grown SiO₂. Ohmic contacts are made by defining highly doped n⁺⁺ regions by phosphorus-ion implantation. We use an overlapping gate integration scheme [28] and use palladium (Pd) gates, which have the beneficial property of small grain size [29]. The gates are electrically isolated by an Al₂O₃ layer grown by atomic layer deposition. The sample is annealed at 400 °C in a hydrogen atmosphere to repair e-beam induced damage to the silicon oxide and to reduce the charge trap density [30, 31].

Figure 1b shows the current through the SET, electrostatically defined using gates ST, LB and RB, which is used as charge sensor and as an electron reservoir. The highly regular peak spacing indicates a well defined quantum dot with a constant charging energy. We form a double quantum dot between the confinement barriers CL and CR, using the gates P₁ and P₂ to tune the quantum dot potentials. B_t and B_R are used to control the tunnel coupling between the quantum dots and from the quantum dots to the SET, respectively.

We characterize the charge readout sensitivity by recording the random telegraph signal (RTS) originating from the tunneling of the electrons between the (2,0) and

* These authors contributed equally to this work.

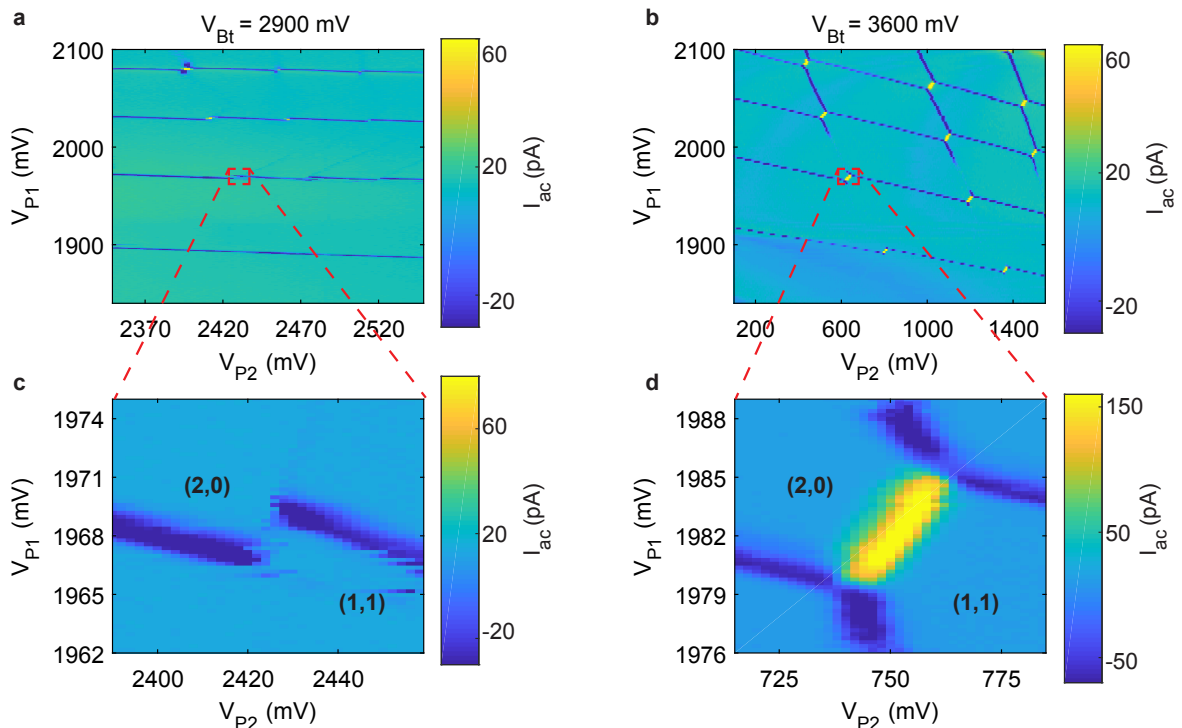


Figure 2. Double quantum dot charge stability diagrams. **a, b** Charge stability diagrams of the charge sensor response I_{ac} as a function of voltages V_{P2} and V_{P1} of a double quantum dot for weak (**a**, $V_{Bt} = 2.9$ V) and strong (**b**, $V_{Bt} = 3.6$ V) coupling. Electrons are loaded from the SET. Transitions with a tunnel rate $\Gamma < f_{ac}$ are not visible. **c, d** High resolution zoom in of the $(2,0)$ - $(1,1)$ anticrossing in for both weak (**c**) and strong (**d**) tunnel coupling.

in the location of D_2 toward the gate P_1 , to a position partly below the gate B_t . This change of quantum dot location will decrease the lever arm and this is likely the cause of the increase in ΔV_{P2} . We conclude that tuning from weak to strong coupling causes the location of D_2 to change from a position mostly under P_2 to a position partly below B_t , while D_1 is stationary under P_1 .

By reducing V_{BR} , the tunnel rate Γ_R between the the SET reservoir and the quantum dots can be reduced and the loading and unloading of electrons can be prevented, resulting in an isolated quantum dot system [26, 32]. Because the reservoir is connected to room temperature electronics, decoupling the quantum dot from it may provide the advantage of reduced noise [33]. Figure 3a shows the $(2,0)$ - $(1,1)$ and $(1,1)$ - $(0,2)$ anticrossings as a function of V_{P2} and V_{P1} for strong coupling. Only inter-dot transition lines are present over a wide range of voltages, much larger than the ΔV_P extracted in the previous section. This implies that no additional electrons are loaded, as a result of a negligible coupling to the reservoir. The ability to control the inter-dot transitions of a double quantum without loading additional electrons provides good prospects for the operation of quantum dot arrays that are only remotely coupled to reservoirs as proposed in quantum information architectures [19, 21, 22].

We control the tunnel coupling t_c with the gate B_T . To compensate for the influence of V_{Bt} on detuning ϵ and on-

site potential U , we implement virtual gates using a cross-capacitance matrix [34] and convert V_{P2} , V_{P1} and V_{Bt} to ϵ , U and t_c . Figure 3b shows the $(2,0)$ - $(1,1)$ and $(1,1)$ - $(0,2)$ anticrossings as a function of the new set of virtual gates V_ϵ and V_{t_c} . For both the transitions the inter-dot line vanishes at low V_{t_c} , meaning that the coupling has been largely switched off. We observe that for the $(1,1)$ - $(0,2)$ anticrossing, the transition line disappears at $V_{t_c} < 3.1$ V, while for the $(2,0)$ - $(1,1)$ anticrossing this happens for $V_{t_c} < 2.95$ V. The variation may come from a small asymmetry in the system.

We tune the double quantum dot to a significantly coupled regime and quantitatively analyze the system by taking charge polarization lines. Figure 3c shows charge polarization lines at high, intermediate and relatively low tunnel couplings within this regime. We measure the charge sensor response V as a function of detuning ϵ and fit the data according to a model that includes cross-talk of ϵ to the charge sensor and the influence of the charge state on the charge sensor sensitivity [9, 35]. From the thermal broadening of the polarization line at low tunnel coupling, we extract the lever arm of V_ϵ for the detuning axis $\alpha_\epsilon \approx 0.04$ eV/mV, by assuming the electron temperature to be equal to the fridge temperature of 0.44 K. Figure 3d shows a t_c proportional to V_{t_c} from approximately 3 to 13 GHz, demonstrating tunable tunnel coupling in the strong coupling regime.

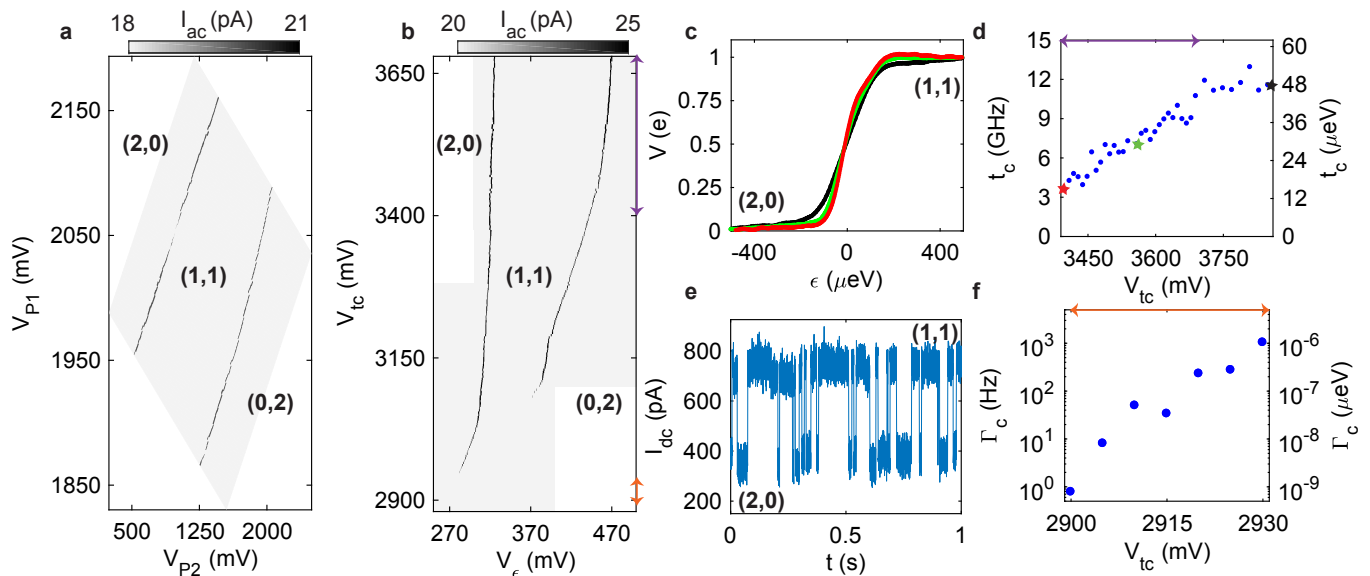


Figure 3. Demonstration of tunable tunnel coupling. **a** Map of the isolated (2,0)-(1,1) and (1,1)-(0,2) anticrossings as a function of V_{P2} and V_{P1} . No additional electrons are loaded into the quantum dot islands due to a negligible Γ_R . **b** Map of the (2,0)-(1,1) and (1,1)-(0,2) anticrossings as a function of detuning and barrier voltage. The relative lever arm between V_{tc} and V_ϵ changes at lower barrier voltages, due to a change in quantum dot location. The orange and purple arrows indicate the regime in which the tunnel coupling was determined using RTS and polarisation line measurements respectively. **c** Polarization lines (excess charge V as a function of detuning ϵ) across the anticrossing for high t_c (black, $V_{tc} = 3.85$ V), intermediate t_c (green, $V_{tc} = 3.6$ V) and relatively low t_c (red, $V_{tc} = 3.4$ V). **d** Extracted t_c from polarization lines as a function of V_{tc} , where we find tunable t_c up to 13 GHz. **e** RTS for weak coupling $V_{tc} = 2.910$ V. **f** Extracted Γ_c from RTS measurements as a function of V_{tc} demonstrating tunable tunnel rates down to below 1 Hz.

At lower tunnel couplings, the thermal broadening of the polarization line prevents accurate fitting. Instead, to obtain the inter-dot tunnel rate Γ_c , we measure RTS (Fig. 3e) at the (2,0)-(1,1) transition and fit the counts C of a histogram of the tunnel times T to $C = Ae^{-\Gamma_c T}$, where A is a constant to normalise the counts. Furthermore we tune the system to be in the elastic tunneling regime, with V_ϵ such that $\Gamma_{c(2,0)-(1,1)} \approx \Gamma_{c(1,1)-(2,0)}$ [36]. This tunnel rate is proportional to the tunnel coupling, but in the weak coupling regime, $\Gamma_c \neq t_c$ due to localisation of the charge [37–39]. Figure 3f shows the obtained Γ_c as a function of V_{tc} from 1 kHz down to below 1 Hz. We note that we can further reduce this tunnel rate to even smaller rates simply by further reducing the gate voltage.

II. DISCUSSION

We have demonstrated control over the tunnel coupling of a double quantum dot in silicon. The inter-dot coupling of the (2,0)-(1,1) charge transition can be controlled by a barrier gate which changes quantum dot location. We have demonstrated control over the tunnel coupling in the strong coupling regime from 3 to 13 GHz, as well as control over the tunnel rate in the weak coupling regime from 1 kHz to below 1 Hz. Achieving this degree of control in an isolated system constitutes a crucial step toward independent control over detuning and tunnel cou-

pling for operation at the charge symmetry point [5, 6], and reaching the control required for large-scale quantum computation with quantum dots [1, 19–24]. While SiMOS systems are often said to be severely limited by disorder, the excellent control shown here provides great prospects to operate larger arrays fabricated using conventional semiconductor technology.

III. METHODS

A. Fabrication

The sample is fabricated on an industrial 300 mm ^{28}Si wafer substrate. The device consists of a highly resistive n-doped silicon substrate, 1 μm of intrinsic natural silicon, a 100 nm thick ^{28}Si epilayer with 800 ppm residual ^{29}Si , covered by 10 nm of thermally grown SiO_2 . We define highly doped n^{++} regions by P-ion implantation, activated by an anneal of 30 seconds at 1000 $^\circ\text{C}$ in a N_2 atmosphere. Ohmic contacts to the silicon are made by electron beam evaporation of 5/55 nm titanium/platinum after locally etching the silicon oxide in buffered hydrogen fluoride. Three gate layers are defined using 100 keV electron beam lithography, electron beam evaporation and liftoff of palladium (17-37-37 nm) with a titanium sticking layer (3-3-3 nm). After each gate layer we grow 7 nm of Al_2O_3 by atomic layer deposition. To

provide a suitable stack for protection during wire bonding, we locally etch the Al_2O_3 and deposit aluminum bondpads with a thickness of $1\ \mu\text{m}$ on top of our gate metal. Finally, the sample is annealed at for 30 minutes at $400\ \text{°C}$ in a forming gas atmosphere.

B. Experimental setup

Gates ST, LB, RB, BR, and CR are connected to low-frequency lines with a cutoff frequency of 30 Hz, while source and drain contacts are connected to fast lines with a cutoff frequency of 150 kHz. Using battery powered voltage sources we apply dc-voltages to the gates. Gates P_2 , B_t and P_1 and CL are connected to bias tees on the printed circuit board to enable simultaneous application of ac and dc signals. Two channels of an arbitrary wave generator (Tektronix AWG5014C) are used to generate ac pulses on fast gates. A Spectrum M4i.4421 digitizer card is used to readout dc and transient signals and an SR 830 lock-in amplifier is used to apply ac excitations and measure charge sensing signals. All measurements have

been performed in a fridge with a base temperature of 0.44 K at a magnetic field of 0 T. Data has been acquired and analyzed using the open source python packages QCoDeS available at <https://qcodes.github.io/Qcodes> and QTT (Quantum Technology Toolbox) available at <https://github.com/QuTech-Delft/qtt>.

C. Acknowledgements

H.G.J.E, L.P and M. V. are funded by a Netherlands Organization of Scientific Research (NWO) VIDI grant. Research was sponsored by the Army Research Office (ARO) and was accomplished under Grant No. W911NF-17-1-0274. The views and conclusions contained in this document are those of the authors and should not be interpreted as representing the official policies, either expressed or implied, of the Army Research Office (ARO), or the U.S. Government. The U.S. Government is authorized to reproduce and distribute reprints for Government purposes notwithstanding any copyright notation herein.

-
- [1] D. Loss and D. P DiVincenzo. Quantum computation with quantum dots. *Physical Review A*, 57(1):120, 1998.
 - [2] J. Levy. Universal quantum computation with spin-1/2 pairs and Heisenberg exchange. *Physical Review Letters*, 89(14):147902, 2002.
 - [3] D. P. DiVincenzo, D. Bacon, J. Kempe, G. Burkard, and K. B. Whaley. Universal quantum computation with the exchange interaction. *Nature*, 408(6810):339, 2000.
 - [4] Z. Shi, C. B. Simmons, J. R. Prance, J. K. Gamble, T. S. Koh, Y.-P. Shim, X. Hu, D. E. Savage, M. G. Lagally, M. A. Eriksson, et al. Fast hybrid silicon double-quantum-dot qubit. *Physical review letters*, 108(14):140503, 2012.
 - [5] F. Martins, F. K. Malinowski, P. D. Nissen, E. Barnes, S. Fallahi, G. C. Gardner, M. J. Manfra, C. M. Marcus, and F. Kuemmeth. Noise suppression using symmetric exchange gates in spin qubits. *Physical review letters*, 116(11):116801, 2016.
 - [6] M. D. Reed, B. M. Maune, R. W. Andrews, M. G. Borselli, K. Eng, M. P. Jura, A. A. Kiselev, T. D. Ladd, S. T. Merkel, I. Milosavljevic, et al. Reduced sensitivity to charge noise in semiconductor spin qubits via symmetric operation. *Physical review letters*, 116(11):110402, 2016.
 - [7] J. M. Taylor, V. Srinivasa, and J Medford. Electrically protected resonant exchange qubits in triple quantum dots. *Physical review letters*, 111(5):050502, 2013.
 - [8] D. Kim, Z. Shi, C. B. Simmons, D. R. Ward, J. R. Prance, T. S. Koh, J. K. Gamble, D. E. Savage, M. G. Lagally, M. Friesen, et al. Quantum control and process tomography of a semiconductor quantum dot hybrid qubit. *Nature*, 511(7507):70, 2014.
 - [9] T. Hensgens, T. and Fujita, L. Janssen, X. Li, C. J. Van Diepen, C. Reichl, W. Wegscheider, S. Das Sarma, and L. M. K. Vandersypen. Quantum simulation of a Fermi–Hubbard model using a semiconductor quantum dot array. *Nature*, 548(7665):70, 2017.
 - [10] M. G. Borselli, K. Eng, R. S. Ross, T. M. Hazard, K. S. Holabird, B. Huang, A. A. Kiselev, P. W. Deelman, L. D. Warren, I. Milosavljevic, et al. Undoped accumulation-mode Si/SiGe quantum dots. *Nanotechnology*, 26(37):375202, 2015.
 - [11] D. M. Zajac, A. J. Sigillito, M. Russ, F. Borjans, J. M. Taylor, G. Burkard, and J. R. Petta. Resonantly driven CNOT gate for electron spins. *Science*, 359(6374):439–442, 2018.
 - [12] N. W. Hendrickx, D. P. Franke, A. Sammak, M. Kouwenhoven, D. Sabbagh, L. Yeoh, R. Li, M. L. V. Tagliaferri, M. Virgilio, G. Capellini, et al. Gate-controlled quantum dots and superconductivity in planar germanium. *Nature communications*, 9(1):2835, 2018.
 - [13] N. W. Hendrickx, D. P. Franke, A. Sammak, G. Scappucci, and M. Veldhorst. Fast two-qubit logic with holes in germanium. *arXiv preprint arXiv:1904.11443*, 2019.
 - [14] D. Sabbagh, N. Thomas, J. Torres, R. Pillarisetty, P. Amin, H. C. George, K. J. Singh, A. Budrevich, M. Robinson, D. Merrill, et al. Wafer-scale silicon for quantum computing. *arXiv preprint arXiv:1810.06521*, 2018.
 - [15] V. Mazzocchi, P.G. Sennikov, A. D. Bulanov, M. F. Churbanov, B. Bertrand, L. Hutin, J. P. Barnes, M. N. Drozdov, J. M. Hartmann, and M. Sanquer. 99.992% ^{28}Si CVD-grown epilayer on 300 mm substrates for large scale integration of silicon spin qubits. *Journal of Crystal Growth*, 509:1–7, 2019.
 - [16] R. Maurand, X. Jehl, D. Kotekar-Patil, A. Corna, H. Bohuslavskiy, R. Laviéville, L. Hutin, S. Barraud, M. Vinet, M. Sanquer, et al. A CMOS silicon spin qubit. *Nature Communications*, 7:13575, 2016.

- [17] M. Veldhorst, C. H. Yang, J. C. C. Hwang, W. Huang, J. P. Dehollain, J. T. Muhonen, S. Simmons, A. Laucht, F. E. Hudson, K. M. Itoh, et al. A two-qubit logic gate in silicon. *Nature*, 526(7573):410–414, 2015.
- [18] W. Huang, C. H. Yang, K. W. Chan, T. Tanttu, B. Hensen, R. C. C. Leon, M. A. Fogarty, J. C. C. Hwang, F. E. Hudson, K. M. Itoh, et al. Fidelity benchmarks for two-qubit gates in silicon. *Nature*, 569:532–536, 2019.
- [19] M Veldhorst, H. G. J. Eenink, C. H. Yang, and A. S. Dzurak. Silicon CMOS architecture for a spin-based quantum computer. *Nature Communications*, 8(1):1766, 2017.
- [20] L. M. K. Vandersypen, H. Bluhm, J. S. Clarke, A. S. Dzurak, R. Ishihara, A. Morello, D. J. Reilly, L. R. Schreiber, and M. Veldhorst. Interfacing spin qubits in quantum dots and donors—hot, dense, and coherent. *npj Quantum Information*, 3(34), 2017.
- [21] R. Li, L. Petit, D. P. Franke, J. P. Dehollain, J. Helsen, M. Steudtner, N. K. Thomas, Z. R. Yoscovits, K. J. Singh, S. Wehner, et al. A crossbar network for silicon quantum dot qubits. *Science advances*, 4(7):eaar3960, 2018.
- [22] J. M. Taylor, H.-A. Engel, W. Dür, A. Yacoby, C. M. Marcus, P. Zoller, and M. D. Lukin. Fault-tolerant architecture for quantum computation using electrically controlled semiconductor spins. *Nature Physics*, 1(3):177, 2005.
- [23] M. Friesen, A. Biswas, X. Hu, and D. Lidar. Efficient multiqubit entanglement via a spin bus. *Physical review letters*, 98(23):230503, 2007.
- [24] B. Trauzettel, D. V. Bulaev, D. Loss, and G. Burkard. Spin qubits in graphene quantum dots. *Nature Physics*, 3(3):192, 2007.
- [25] N. S. Lai, W. H. Lim, C. H. Yang, F. A. Zwanenbourg, W. A. Coish, F. Qassemi, A. Morello, and A. S. Dzurak. Pauli spin blockade in a highly tunable silicon double quantum dot. *Scientific reports*, 1(110), 2011.
- [26] C. H. Yang, R. C. C. Leon, J. C. C. Hwang, A. Saraiva, T. Tanttu, W. Huang, J. Camirand Lemyre, K. W. Chan, K. Y. Tan, F. E. Hudson, et al. Silicon quantum processor unit cell operation above one Kelvin. *arXiv preprint arXiv:1902.09126*, 2019.
- [27] M. Veldhorst, J. C. C. Hwang, C. H. Yang, A. W. Leenstra, B. de Ronde, J. P. Dehollain, J. T. Muhonen, F. E. Hudson, K. M. Itoh, A. Morello, et al. An addressable quantum dot qubit with fault-tolerant control-fidelity. *Nature Nanotechnology*, 9(12):981–985, 2014.
- [28] S. J. Angus, A. J. Ferguson, A. S. Dzurak, and R. G. Clark. Gate-defined quantum dots in intrinsic silicon. *Nano Letters*, 7(7):2051–2055, 2007.
- [29] M. Brauns, S. V. Amitonov, P. C. Spruijtenburg, and F. A. Zwanenbourg. Palladium gates for reproducible quantum dots in silicon. *Scientific reports*, 8(1):5690, 2018.
- [30] J. S. Kim, A. M. Tyryshkin, and S. A. Lyon. Annealing shallow Si/SiO₂ interface traps in electron-beam irradiated high-mobility metal-oxide-silicon transistors. *Applied Physics Letters*, 110(12):123505, 2017.
- [31] E. P. Nordberg, G. A. Ten Eyck, H. L. Stalford, R. P. Muller, R. W. Young, K. Eng, L. A. Tracy, K. D. Childs, J. R. Wendt, R. K. Grubbs, et al. Enhancement-mode double-top-gated metal-oxide-semiconductor nanostructures with tunable lateral geometry. *Physical Review B*, 80(11):115331, 2009.
- [32] Benoit Bertrand, Hanno Flentje, Shintaro Takada, Michihisa Yamamoto, Seigo Tarucha, Arne Ludwig, Andreas D Wieck, Christopher Bäuerle, and Tristan Meunier. Quantum manipulation of two-electron spin states in isolated double quantum dots. *Physical review letters*, 115(9):096801, 2015.
- [33] A. Rossi, T. Ferrus, and D. A. Williams. Electron temperature in electrically isolated Si double quantum dots. *Applied Physics Letters*, 100(13):133503, 2012.
- [34] T. A. Baart, M. Shafiei, T. Fujita, C. Reichl, W. Wegscheider, and L. M. K. Vandersypen. Single-spin CCD. *Nature Nanotechnology*, 11(4):330, 2016.
- [35] L. DiCarlo, H. J. Lynch, A. C. Johnson, L. I. Childress, K. Crockett, C. M. Marcus, M. P. Hanson, and A. C. Gossard. Differential charge sensing and charge delocalization in a tunable double quantum dot. *Physical review letters*, 92(22):226801, 2004.
- [36] S. Tarucha, T. Fujisawa, K. Ono, D. G. Austing, T. H. Oosterkamp, W. G. van der Wiel, and L. P. Kouwenhoven. Elastic and inelastic single electron tunneling in coupled two dot system. *Microelectronic engineering*, 47(1-4):101–105, 1999.
- [37] F. R. Braakman, P. Barthelemy, C. Reichl, W. Wegscheider, and L. M. K. Vandersypen. Long-distance coherent coupling in a quantum dot array. *Nature Nanotechnology*, 8(6):432, 2013.
- [38] J. K. Gamble, M. Friesen, S. N. Coppersmith, and X. Hu. Two-electron dephasing in single Si and GaAs quantum dots. *Physical Review B*, 86(3):035302, 2012.
- [39] A. N. Korotkov. Continuous quantum measurement of a double dot. *Physical Review B*, 60(8):5737, 1999.